Effect of top-cell CGS thickness on the performance of CGS/CIGS tandem solar cell

ARTICLE *in* SOLAR ENERGY · AUGUST 2015

Impact Factor: 3.47 · DOI: 10.1016/j.solener.2015.08.029

3 AUTHORS, INCLUDING:

Souad Tobbeche

10 PUBLICATIONS **18** CITATIONS

SEE PROFILE

Amar Merazga

Taif University

41 PUBLICATIONS **98** CITATIONS

SEE PROFILE

Available online at www.sciencedirect.com

ScienceDirect

Solar Energy 122 (2015) 104–112

SOLAR ENERGY

www.elsevier.com/locate/solener

Effect of top-cell CGS thickness on the performance of CGS/CIGS tandem solar cell

M. Elbar [a], S. Tobbeche [a,*], A. Merazga [b]

[a] *Laboratoire des matériaux semiconducteurs et métalliques (LMSM), Faculté des Sciences et de la Technologie, Département de Génie-Electrique, Université de Biskra, BP 145, 07000 Biskra, Algeria*

[b] *Physics Department, Faculty of Science, Taif University, Taif 21974, Saudi Arabia*

Received 26 June 2015; received in revised form 3 August 2015; accepted 20 August 2015

Communicated by: Associate Editor Nicola Romeo

Abstract

The photovoltaic characteristics of a double junction CGS/CIGS tandem solar cell, based on copper gallium diselenide (CGS) and copper indium gallium diselenide (CIGS) structures as top-cell and bottom-cell respectively, were numerically simulated under AM1.5 G spectral illumination using the two-dimensional device simulator Silvaco–Atlas. The performance of single CGS and CIGS solar cells with fixed thicknesses at 0.26 μm and 3.5 μm, respectively, were simulated first. They present conversion efficiencies of 18.92% and 20.32% respectively, in good agreement with experimental high record efficiencies found in literature. Maintaining the thickness of the bottom CIGS cell at 3.5 μm, the top-cell CGS thickness dependence of the tandem cell performance is then investigated within the range from 0.10 μm to 0.28 μm. The optimal thickness corresponding to maximum conversion efficiency of 26.21% is 0.19 μm. This thickness of the top-cell coincides well with the point of "current matching" where the short-circuit current densities of the top, bottom and tandem cells are exactly equal to one another and equal to 18.06 mA/cm^2, which is also maximum short-circuit current density of the tandem cell at the optimal top-cell thickness 0.19 μm. Thickness dependent light absorption of the top-cell CGS layer is the main reason for this efficiency improvement.

Keywords: CGS solar cell; CIGS solar cell; CGS/CIGS tandem solar cell; CGS thickness; Current matching

1. Introduction

Thin-film solar cells have the potential for low-cost and large-scale photovoltaic applications. A number of semiconductor materials, such as amorphous silicon (a-Si:H), polycrystalline cadmium telluride (CdTe) and copper indium gallium diselenide (CIGS) for example, have been used for thin-film photovoltaic solar cells. The CIGS compound material is a semiconductor with a suitable energy band-gap of high optical absorption coefficient in the visible spectrum of sunlight. The absorption coefficient of CIGS film in the visible spectrum is, in fact, 100 times higher than that of the silicon film. Furthermore, the CIGS thin-film solar cell exhibits an excellent outdoor stability and radiation hardness and achieves the highest conversion efficiency compared to other chalcopyrite and compared to CdTe and a-Si:H thin-film solar cells. A single-junction thin-film CIGS solar cell with an active area of 0.5 cm^2 exhibited the highest efficiency of 20.3% at the "Centre of Solar Energy and Hydrogen Research Baden-Württemberg" (ZSW) (Jackson et al., 2011) and 19.9% at

* Corresponding author. Tel.: +213 7 96 55 85 09.
E-mail address: souad_tobbeche@yahoo.fr (S. Tobbeche).

http://dx.doi.org/10.1016/j.solener.2015.08.029
0038-092X/

the National Renewable Energy Laboratory (NREL) (Repins et al., 2008b). Single junction thin-film solar cells have the advantages of low cost (Marika, 2012) and high efficiency (Repins et al., 2008a) compared to other solar cells, but their efficiencies are constrained by the Shockley Queisser limit (Shockley and Queisser, 1961). Further efficiency improvement requires the use of multi-junction configurations (Green, 2001). Crystalline multi-junction solar cells hold the world record efficiency (Green et al., 2013), but they are expensive to produce due to the need of expensive epitaxial growth (Cotal et al., 2009). It would then be desirable to use multi-junction solar cells based on low-cost polycrystalline thin-films such as CdTe and CIGS. The band-gap energy of the $CuIn_{(1-x)}Ga_xSe_2$ (CIGS) films varies in the range from 1.04 eV to 1.68 eV with the corresponding Ga proportion ranging from $x = 0$ to $x = 1$ (Huang, 2008). CIGS is, therefore, a prime candidate for application in multi-junction solar cells. An increase in efficiency is expected by using the denominated tandem multi-junction solar cells, consisting of layers with different band-gap energies in order to exploit different energy regions of the solar spectrum. Tandem solar cells consist of a large band-gap top-cell, which absorbs the short wavelength (high energy) part of the solar spectrum, and a low band-gap bottom-cell absorbing in the longer wavelength range. The top-cell should be transparent below the band-gap of its absorber and connected to the bottom-cell via a transparent conducting layer. For CIGS solar cells, $MoSe_2$ on ZnO, SnO_2:F, In_2O_3:Sn and ZnO can be used as connection materials because they make good ohmic contacts with the CIGS absorber. When two solar cells are stacked monolithically, a reverse biased p–n junction forms at their interface and tunnel junction diodes are typically used in between to solve this reverse bias problem. In this context, modeling and simulation of a CGS/CIS tandem solar cell with a p-Cu_2O/n-In_2O_3 broken-gap tunnel junction resulted in an efficiency of 24.1% (Song et al., 2015). The modeled efficiency for a CGS/CIGS tandem cell was 25% (Jiyon et al., 2003) and for a CdZnTe/CIGS tandem cell the modeled efficiency was 26% (Xiao et al., 2010). Modeling of a low-cost organic/inorganic hybrid tandem cell to achieve efficiencies exceeding 20% have also been reported (Beiley et al., 2012). The development of mechanically stacked and monolithically integrated tandem cells using CIGS as bottom-cell and a dye-sensitized solar cell (DSSC) as top-cell, with different methods to increase the transmittance of the DSSC top-cell, is also an active issue (Seyrling et al., 2009). The DSSC/CIGS tandem cell was first made by Gratzel yielding conversion efficiency greater than 15% (Liska et al., 2006), 12.35% (Jeong et al., 2011) and 10.46% (Wang et al., 2010). The tandem solar cell employs two sub-cells connected in a serial structure. When this serial configuration is used, it is expected that the open-circuit voltage V_{oc} of the tandem cell is equal to the sum of V_{oc} of each sub-cell (Olson et al., 2003). Mechanically stacked tandem cells based on Ag(In, Ga)Se_2 (AIGS) as top-cell and CIGS as bottom-cell presented open-circuit voltages as high as 1.5 V (Nakada et al., 2006). Having CIGS as bottom-cell, the band-gap 1.68 eV of the $CuGaSe_2$ (CGS) cell satisfies ideally the requirements for a top-cell to form with the CIGS cell an ideal CGS/CIGS tandem cell. The Series-connected CGS/CIGS tandem cell was reported to achieve a high open-circuit voltage of 1.18 V with a conversion efficiency of 7.4% (Nishiwaki et al., 2003). It had been conjectured that the current density of the serial tandem cell is limited to the current density of the sub-cell showing the lower current density (Burdick and Glatfelter, 1986) and that the current density mismatch between the sub-cells may induce a significant current loss in the corresponding tandem cell (Jun et al., 2009).

In order to fully exploit the opportunity offered by the tandem structure, we propose in the present work to use the cell thickness as adjustable parameter in order to tune the short-circuit current density and search the "current matching" point at which the top and bottom-cells share the same short-circuit current density. We have used the Silvaco–Atlas software (ATLAS, 2015) to design and study the single CGS and CIGS and the tandem CGS/CIGS solar cells as a function of the CGS top-cell thickness. In the first step, we will report the modeling and simulation results of the single CGS and CIGS solar cells and compare them to related previously reported experimental results. In the second step, we will show the simulation results of the tandem CGS/CIGS solar cell with CGS as top-cell absorber and CIGS as bottom-cell absorber. The CGS/CIGS tandem cell exhibited an improvement in photovoltaic performance compared to the single CGS and CIGS solar cells. Current matching was shown to be the prerequisite condition for optimization of the CGS/CIGS tandem cell performance at maximum efficiency. This was achieved by adjusting the CGS top-absorber thickness to an optimal value where the short-circuit current densities of the top, bottom and tandem cells are similar. The role of current matching in the improvement of the CGS/CIGS tandem cell performance was simulated and analyzed.

2. Tandem cell structure and numerical simulation

High efficiencies could be obtained by stacking together different absorbers with different band-gaps to maximize the light absorption. The basic structure of the CGS/CIGS tandem solar cell is shown in Fig. 1. It consists of two solar cells: The CGS wide band-gap ($E_g = 1.69$ eV) top-cell having a small adjustable thickness and the CIGS low band-gap ($E_g = 1.16$ eV) bottom-cell with a normal thickness of 3.5 μm (Jackson et al., 2011). This design is intended to convert a wide range of incident photons on the solar cell and generate a maximum power output. The detailed design of this tandem cell consists of a top n-CdS/p-CGS hetero-junction and a bottom n-CdS/p-CIGS hetero-junction, which are optically and electrically connected through a ZnO-layer serving as a transparent conducting oxide (TCO). The tandem cell was considered to be illuminated under AM1.5 G solar spectrum with 100 mW/cm^2 incident

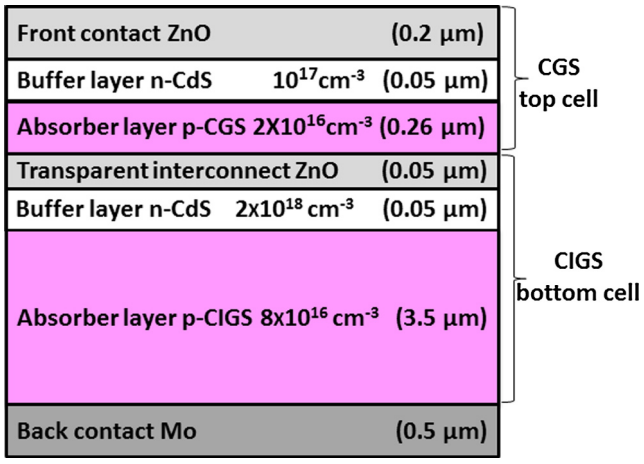

Fig. 1. Schematic structure of the simulated tandem solar cell with CGS/CIGS sub-cells connected by transparent interconnect ZnO, the relative doping concentrations and the thicknesses are listed for each layer.

power density. The solar radiation was assumed to be normally incident on the ZnO-layer which represents the front cathode contact for the back anode contact represented by a molybdenum (Mo) layer. The doping concentrations and different thicknesses used in the simulation are indicated in Fig. 1. Silvaco–Atlas 2D simulator was used to develop the numerical simulations for the designed CGS and CIGS solar cells on the basis of the drift–diffusion transport model. The latter consists of a set of fundamental equations including Poisson's equation, the continuity equations and the transport equations. Poisson's equation relates variations in electrostatic potential to local charge densities. The continuity and transport equations describe the way that electron and hole densities evolve as a result of generation, recombination and transport processes.

3. Simulation parameters

The 2D Silvaco Atlas simulator requires input of the device parameters related to each layer and material in the cell structure (Tables 1–3). Solar cells based on $CuIn_{1-x}Ga_xSe_2$ absorber are particularly attractive since the device parameters can be changed by changing the stoichiometry (composition x) of the absorber material. $CuIn_{1-x}Ga_xSe_2$ is a direct band-gap material with the band-gap energy E_g dependent on the composition ratio $x = Ga/(In + Ga)$. It has been established that as a function of x the band-gap can be determined from the relation given in (Fotis, 2012) as

$$E_g(x) = 1.011 + 0.664x - 0.249(1 - x) \quad (1)$$

where E_g ranges from 1.011 eV to 1.69 eV for x ranging from 0 for CIS to 1 for CGS respectively.

The electron (μ_n) and hole (μ_p) mobilities of each layer were set according to Amin et al., (2007) and Gloeckler et al. (2003). The electron affinity χ_e of the material $CuInGaSe_2$ was reported to be in the range of 4.10–4.90 eV (Hunger et al., 2001) and 4.8 eV was selected for the present simulation. The conduction and valence band effective densities of states N_c and N_v were set according to Shang et al. (2014) for each layer. All the layers are polycrystalline and therefore contain a large number of defects (Ouédraogo et al., 2014). According to Scheer (2011), we considered two Gaussian deep donor defect distributions for the CGS and CIGS layers and a Gaussian deep acceptor defect distribution for the CdS layer. The acceptor and donor defect distributions are given by (ATLAS, 2015; Jankovic, 2012):

$$g_{GA}(E) = N_{GA} \exp\left(-\left(\frac{E_{GA} - E}{W_{GA}}\right)^2\right) \quad (2)$$

$$g_{GD}(E) = N_{GD} \exp\left(-\left(\frac{E - E_{GD}}{W_{GD}}\right)^2\right) \quad (3)$$

where E is the defect energy, the subscripts (G, A, D) stand for Gaussian, acceptor and donor defect states, respectively. The density of states is characterized by the effective density of states N_{GA} or N_{GD}, the standard energy deviation W_{GA} or W_{GD}, and the peak energy position E_{GA} or E_{GD}. The position of the recombinative defect states lies in a narrow distribution close to the middle of the band-gap (Scheer, 2011; Gloeckler et al., 2003). Shockley–Read–Hall (SRH) recombination model for the implemented defects in the Silvaco simulator is used to calculate carrier recombination rates which depend on the density of states located through the band-gap, the defect energy position and the electron (σ_n) and hole (σ_p) capture cross sections. For steady-state conditions, the net electron (R_n) and hole (R_p) recombination rates are identical. The SRH recombination rate due to defect states is given by (ATLAS, 2015):

Table 1
Material parameters used in the simulation.

Layer properties	CdS	CGS/CIGS
Layer band gap E_g (eV)	2.4	1.69/1.16
Electron affinity χ_e (eV)	4.5	4.8
Relative permittivity ε_r (F cm^{-1})	10	13.6
Electron mobility μ_n (cm^2/V s)	100	100
Hole mobility μ_p (cm^2/V s)	25	25
Conduction band effective density of states N_c (cm^{-3})	2.2×10^{18}	2.2×10^{18}
Valence band effective density of states N_v (cm^{-3})	1.8×10^{19}	1.8×10^{19}

Table 2
Simulation parameters of defect states densities and electron (hole) capture cross-sections. A and D denote Acceptor and Donor defects.

Gaussian defect states		
Gaussian defect density N_{GA}, N_{GD} (cm^{-3})	10^{15} (A)	10^{15} (D)
Peak energy position E_{GA}, E_{GD} (eV)	1.2 (A)	0.84/0.58 (D)
Standard energy deviation W_{GA}, W_{GD} (eV)	0.1 (A)	0.1 (D)
Electron capture cross section σ_n (cm^2)	10^{-15}	2×10^{-15}
Hole capture cross section σ_p (cm^2)	10^{-17}	3×10^{-13}

Table 3
Simulation parameters of surface recombination velocities of electrons (S_n) and holes (S_p).

Surface recombination velocities for electrons (S_n) and holes (S_p) (cm s^{-1})		
CdS/CIGS interface	10^5	10^5
CdS/CGS interface	10^5	10^5
Front contact	10^5	10^5
Back contact	10^5	10^5

$$R_{n,p} = \int_{E_v}^{E_c} \frac{\sigma_{nA}\sigma_{pA}(np - n_i^2)g_{GA}(E)}{\sigma_{nA}\left(n + n_i \exp\left[\frac{E-E_i}{kT}\right]\right) + \sigma_{pA}\left(p + n_i \exp\left[\frac{E_i-E}{kT}\right]\right)} dE + \int_{E_v}^{E_c} \frac{\sigma_{nD}\sigma_{pD}(np - n_i^2)g_{GD}(E)}{\sigma_{nD}\left(n + n_i \exp\left[\frac{E-E_i}{kT}\right]\right) + \sigma_{pD}\left(p + n_i \exp\left[\frac{E_i-E}{kT}\right]\right)} dE \quad (4)$$

where n and p are the electron and hole concentrations, n_i is the intrinsic carrier concentration, E_i is the Fermi level for intrinsic (undoped) material, k is Boltzmann's constant and T is the temperature.

The capture cross sections σ_n and σ_p can vary between 10^{-17} and 10^{-12} cm^2 (Gloeckler et al., 2003), and were chosen for the present simulation to be 2×10^{-15} cm^2 for σ_n of CGS and CIGS layers and 3×10^{-13} cm^2 for σ_p of CGS and CIGS materials. For CdS, $\sigma_n/\sigma_p = 10^{-15}$ cm^2/10^{-17} cm^2 were selected. Defect recombination at the semiconductor hetero-interfaces (e.g. CdS/CGS, CdS/CIGS) and at the front and back contacts are modeled by inclusion of surface recombination velocities of both electrons (S_n) and holes (S_p) chosen to be similar and equal to 10^5 cm/s. The optical parameters of the real and imaginary parts of the wavelength-dependent refractive index $n(\lambda)$ and extinction coefficient $k(\lambda)$ for the CGS and CIGS materials are obtained from Paulson et al. (2003) and for the ZnO and CdS materials from Richter et al. (2013) and Palik (1998). For the metal contact material Mo, optical constants available in the SOPRA database of the Silvaco–Atlas simulator were used in the present simulation. Reflection loss from the surface of the tandem cell has also been integrated into the model. In this study, the solar cells operating temperature was set at 300 K.

4. Results and discussions

The CIGS and CGS solar cells are first simulated separately using the simulation parameters shown in Tables 1–3.

4.1. Modeling the single CIGS and CGS solar cells

The CIGS bottom-cell is shown in Fig. 2. It is made of a p-type CIGS absorber and an n-type CdS buffer. A TCO layer from ZnO is deposited on top of the cell and back metallization is made from Mo for electrical contacts. The Ga composition is about 0.31, which corresponds to band-gap energy of 1.16 eV. This simulated CIGS cell is similar to that achieved experimentally in (Jackson et al., 2011). The cell structure from bottom to top consists of the following: a soda-lime glass of 3 mm thickness, a

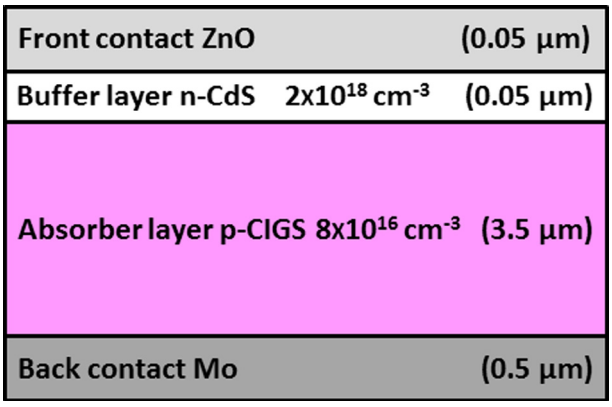

Fig. 2. Single CIGS bottom-cell schematic structure.

sputtered Mo layer of thickness in the range 500–900 nm, the CIGS absorber of thickness between 2.5 µm and 3.5 µm, a chemical bath-deposited CdS buffer layer ranging from 40 nm to 50 nm, a sputtered undoped ZnO layer with a thickness of 50 nm to 100 nm, a sputtered Al-doped ZnO layer with thickness in the range 150–200 nm and a Ni/Al grid for the front electrical contact. CIGS solar cells with efficiency of 20.3% were produced by varying the composition x from 0.30 to 0.35 (Jackson et al., 2011). The doping concentrations of the CdS and CIGS layers are indicated in Fig. 2.

The so-called CGS solar cell structure consists of a p-type CGS absorber, an n-type CdS buffer, a TCO layer from ZnO material deposited on top of the cell and a Mo layer serving for back contact. In Fig. 3 is shown this CGS cell structure. The Ga composition $x = 1$ corresponds to energy band-gap of 1.69 eV. CdS and CGS doping concentrations were optimized to improve the conversion efficiency of the CGS cell.

The simulation results of the J–V characteristics for the single CIGS and CGS solar cells are presented in Fig. 4. The photovoltaic parameters of the single CIGS bottom-cell extracted from the corresponding J–V characteristic are given in Table 4 together with other simulation and experimental results for comparison. It can be seen that the simulation results including the efficiency η of 20.32% are in good agreement with experimentally existing results in literature (Jackson et al., 2011) and are better than those obtained by simulation of a conventional CIGS solar cell with a CdS buffer layer thickness (50 nm) and a CIGS

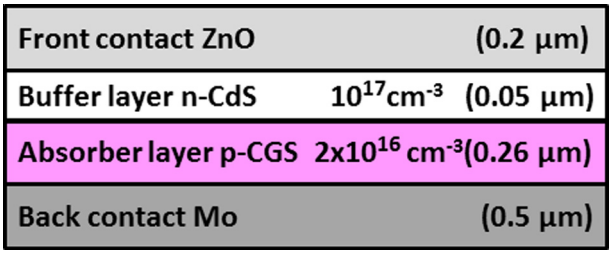

Fig. 3. Single CGS top-cell schematic structure.

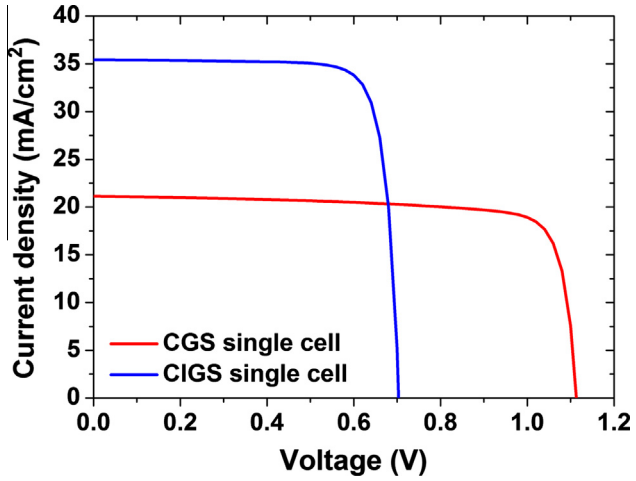

Fig. 4. J–V characteristics for the single CIGS and CGS solar cells.

absorber layer thickness (3.5 μm) using the simulator SCAPS (Chelvanathan et al., 2010), thus validating the model and the parameters chosen for the simulation. The photovoltaic parameters for the single CGS top-cell extracted from the corresponding J–V characteristic are summarized in Table 5. The simulation results show reasonable V_{oc} and FF, but low J_{sc}. The resulting η is 18.92% which is lower than that of the CIGS cell mainly due to lower J_{sc}.

4.2. Modeling the CGS/CIGS tandem cell

The CGS/CIGS tandem solar cell structure is shown in Fig. 1. To model the transparent interconnect ZnO-layer in the tandem cell an approach is used and consists of adding an electrode which exactly overlay the transparent interconnect ZnO-layer and attaching a lumped resistance to it using the "contact name = com resist = 10^{16}" Atlas statement (SILVACO, 2015). In doing this, we force the current to flow from anode to cathode and prevent any current to flow in the added electrode. Physically it can be justified by the fact the interconnect layer is acting like a resistor letting current flows without significant limitation. The value of the resistance can be used to adjust the amount of current allowing to flow through the added electrode thus controlling the interlayer resistance.

The J–V characteristics of the CGS top-cell, the CIGS bottom-cell and the whole CGS/CIGS tandem cell are shown together in Fig. 5. The photovoltaic parameters deduced from these characteristics are indicated in Table 5. To obtain the J–V curves of the top and bottom cells, the

Table 5
Photovoltaic parameters of the top, bottom and tandem solar cells.

	J_{sc} (mA/cm^2)	V_{oc} (V)	FF (%)	η (%)
CGS single cell	21.13	1.11	80.42	18.92
CGS top-cell	20.26	1.11	80.94	18.22
CIGS bottom-cell	16.17	0.69	79.05	8.83
CGS/CIGS tandem cell	16.35	1.8	85.09	25.11

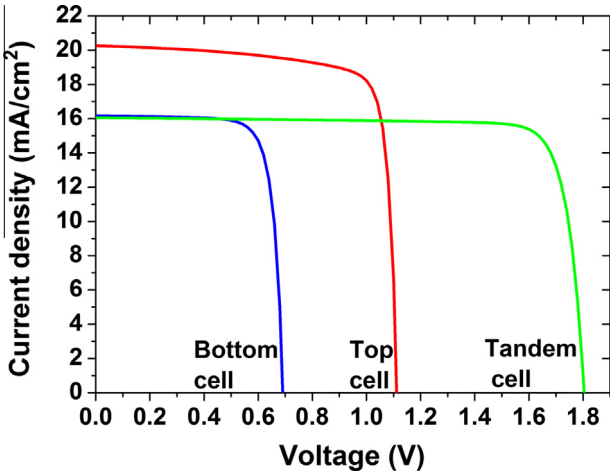

Fig. 5. J–V characteristics for the CGS top-cell, CIGS bottom-cell and CGS/CIGS tandem cell.

anode and cathode contacts of the top-cell were respectively set at the interconnect ZnO-layer and at the front ZnO-layer, whereas the anode and cathode contacts of the bottom-cell were respectively set at the back Mo layer and at the interconnect ZnO-layer. The J_{sc} of the tandem cell is limited by the low current of the CIGS bottom-cell, such that the tandem J_{sc} of 16.35 mA/cm^2 is about equal to the bottom-cell J_{sc} of 16.17 mA/cm^2. On the other hand, the tandem V_{oc} (1.8 V) is exactly equal to the summation of the top-cell V_{oc} (1.11 V) and the bottom-cell V_{oc} (0.69 V). From these results, the correct operation of the series connected CGS and CIGS cells forming the tandem cell is demonstrated. In addition, the fill factor of the tandem cell (85.09%) is higher than those of the top-cell (80.94%) and the bottom-cell (79.05%). Clearly, the increase of V_{oc} and FF of the tandem cell is the cause of the efficiency improvement to 25.11% with respect to those of the single CIGS (20.32%) and CGS (18.92%) cells. Few simulation studies of tandem solar cells based on CGS and CIGS cells are reported. The performance for the CGS/CIGS tandem cell with a double band-gap graded ClGS bottom-cell at various CGS absorber thickness were

Table 4
Simulation and experiment parameters of a CIGS solar cell.

	J_{sc} (mA/cm^2)	V_{oc} (V)	FF (%)	η (%)
CIGS single cell simulation	35.44	0.709	80.69	20.32
CIGS cell simulation (Chelvanathan et al., 2010)	33.5	0.67	80	17.5
Experiment (Jackson et al., 2011)	35.4	0.74	77.5	20.3

numerically studied using AMPS-1D software (Jiyon et al., 2003). The simulation results suggest that it is possible to achieve a 25% conversion efficiency in the CCS/CIGS tandem cell with an optimized CGS and CICS cell structure for the two-junction tandem cell. The optimization of the layers thicknesses and Ga ratio for a CGS/CIGS tandem solar cell using Silvaco–Atlas software leads to an optimum efficiency of 24% (Fotis, 2012). In the present work, the simulated efficiency of 25.11% obtained for the unoptimized GGS/CIGS tandem cell is better than those reported in (Jiyon et al., 2003; Fotis, 2012).

Comparing the results of the CIGS single cell with those of the CIGS bottom-cell in the tandem cell, we observe that the photovoltaic parameters of the CIGS bottom-cell have significantly degraded due to the top layers absorbing some of the incident light. The results of the CGS top-cell in the tandem cell, as compared to those of the CGS single cell, rather show small decreases of the photovoltaic parameters due to smaller light absorption by the bottom layers. The J_{sc} of the tandem cell is limited by the low J_{sc} of the CIGS bottom-cell simply because the top and bottom cells were current-mismatched, resulting in a relatively low tandem cell efficiency.

4.3. Effect of the top-cell CGS thickness

Because the photon energy dependent absorption coefficient $\alpha(h\nu)$ in solar cell materials is not infinite, a solar cell of finite thickness will not absorb all the incident light of photon energy above the band-gap. Some of the incident light will be transmitted (especially at photon energies near the band-gap where α is small). The thinner the cell, the greater is the transmission. Therefore, for a tandem solar cell, decreasing the top-cell thickness will reapportion the light between the two cells, increasing the bottom-cell current at the expense of the top-cell current. Before decreasing the CGS thickness, if the short-circuit current density of the bottom-cell J_{scb} is lower than the short-circuit current density of the top-cell J_{sct}, then the thickness of the top-cell can be reduced to reach the current matching condition where $J_{scb} = J_{sct}$. Because the tandem cell current density J_{sc} is limited to the lower one of J_{scb} and J_{sct}, J_{sc} and hence the cell efficiency will be maximized when the top-cell thickness is decreased to reach this current matching condition. In the present work, we varied the CGS top-cell thickness from 0.1 μm to 0.28 μm in the CGS/CIGS tandem cell with the thickness of the CIGS bottom-cell being fixed at 3.5 μm. The tandem solar cell structure is shown in Fig. 1 and the simulation parameters are indicated in Tables 1–3. In Fig. 6(a) are plotted the short-circuit current densities of the top and bottom cells as a function of the thickness of the CGS layer, where strong dependence is shown for both currents. As the thickness of the CGS layer in the top-cell increases, the top-cell J_{sct} increases and the bottom-cell J_{scb} decreases. This is simply because the thick top-cell absorbs more light, leaving transmitted less light to the bottom-cell and, in contrast, the thin

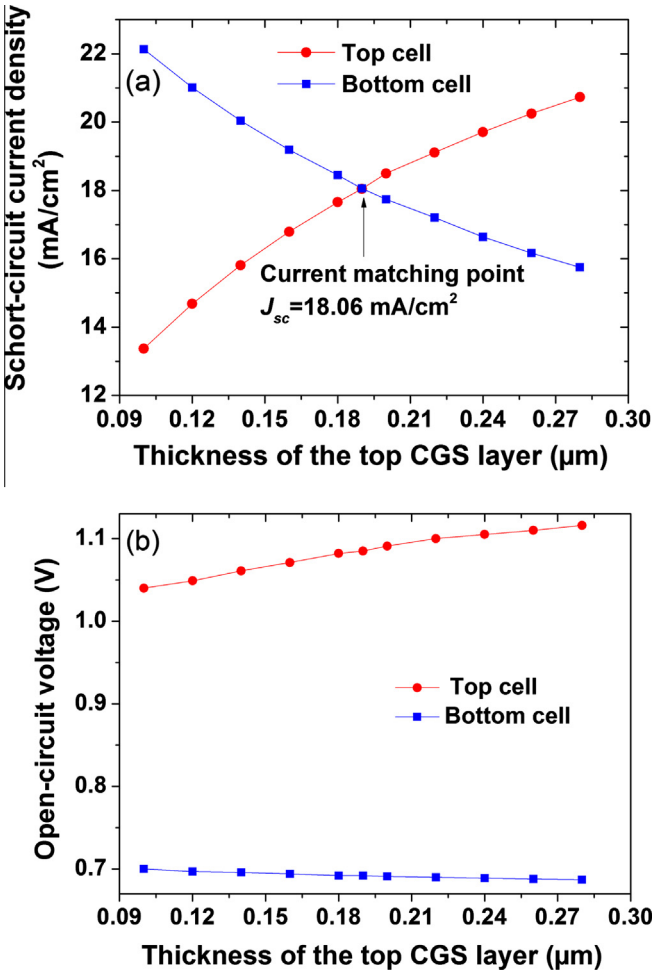

Fig. 6. (a) Short-circuit current densities of the top CGS and bottom CIGS solar cells as a function of the top CGS layer thickness in a CGS/CIGS tandem solar cell and (b) Open-circuit voltages of the top CGS and bottom CIGS solar cells as a function of the top CGS layer thickness in a CGS/CIGS tandem solar cell.

top-cell absorbs less light, leaving transmitted more light to the bottom-cell. With progressive increase of the CGS layer in the top-cell, the increasing J_{sct} and the decreasing J_{scb} cross one another at an optimal CGS thickness of 0.19 μm where the current matching condition $J_{sct} = J_{scb} = 18.06$ mA/cm^2 is fulfilled.

The open-circuit voltages of the top and bottom cells as a function of the top CGS layer thickness are shown in Fig. 6(b). The V_{oc} of the top-cell increases with the CGS layer thickness. This is mainly because that the thicker CGS absorber layer will absorb more photons with longer wavelength, which will in turn make a contribution to the generation of electron–hole pairs. However, the V_{oc} of the bottom-cell is nearly independent of the variation of the CGS layer thickness.

In Fig. 7(a–d) are plotted the simulated photovoltaic parameters of the tandem cell as a function of the CGS layer thickness. The short-circuit current density J_{sc} in Fig. 7(a) shows an increase from 13.48 mA/cm^2 to 18.06 mA/cm^2 with increasing CGS thickness from 0.1 to

0.19 μm. The increased J_{sc} is attributed to enhanced light absorption in the top-cell. Therefore, for the lower range of the CGS layer thickness between 0.1 μm and 0.19 μm, the tandem cell J_{sc} is controlled by the top-cell current J_{sct}, as shown in Fig. 6(a). With further increase of the CGS thickness between 0.19 and 0.28 μm, the tandem cell J_{sc} decreases back from 18.06 mA/cm^2 to 15.93 mA/cm^2. Thus, the tandem cell J_{sc} is controlled by the bottom-cell current J_{scb} in the upper range of the CGS layer thickness, as shown in Fig. 6(a). The tandem cell J_{sc} reaches a maximum 18.06 mA/cm^2 at the optimal CGS layer thickness 0.19 μm, for which the current matching condition $J_{sc} = J_{sct} = J_{scb} = 18.06$ mA/cm^2 is established.

Fig. 7(b) illustrates the dependence of the tandem cell V_{oc} on the CGS layer thickness. The open-circuit voltage increases over the whole range as the CGS thickness increases. In the case of a tandem cell, the open-circuit voltage is the sum of the open-circuit voltages of bottom and top cells. The V_{oc} values of the top-cell are higher than those of the bottom-cell as illustrated in Fig. 6(b). Thus the increase of the top-cell V_{oc} with the CGS layer thickness causes the increase in the tandem cell V_{oc} and consequently the open-circuit voltages of the top and tandem cells present similar increase tendencies with the CGS layer thickness.

In Fig. 7(c), is shown the variation of the tandem cell *FF* with varying CGS layer thickness. In reverse to J_{sc} variation, the *FF* presents a minimum of 81.44% at the optimal CGS thickness 0.19 μm. It starts decreasing from 86.65% at 0.1 μm CGS thickness and then increases back from the minimum 81.44% to reach 85.42% at 0.28 μm.

Finally, in Fig. 7(d) the conversion efficiency η of the tandem cell is plotted against the CGS layer thickness. Similarly to J_{sc}, the tandem cell η presents a maximum of 26.21% at the optimal CGS layer thickness 0.19 μm where the current matching between the top and bottom cells occurs. The tandem cell η starts increasing from 20.32% at 0.1 μm to the maximum 26.21% as the CGS layer thickness increases, and then decreases back from this maximum to about 24.5% at 0.28 μm.

The decrease of *FF* to a minimum at the current matching point slightly undermines the η variation, but the considerable increase of the J_{sc} supported by the increase of the V_{oc} has over-balanced the decrease effect of *FF* on η, providing the η variation with an increasing trend and a maximum at the current matching point.

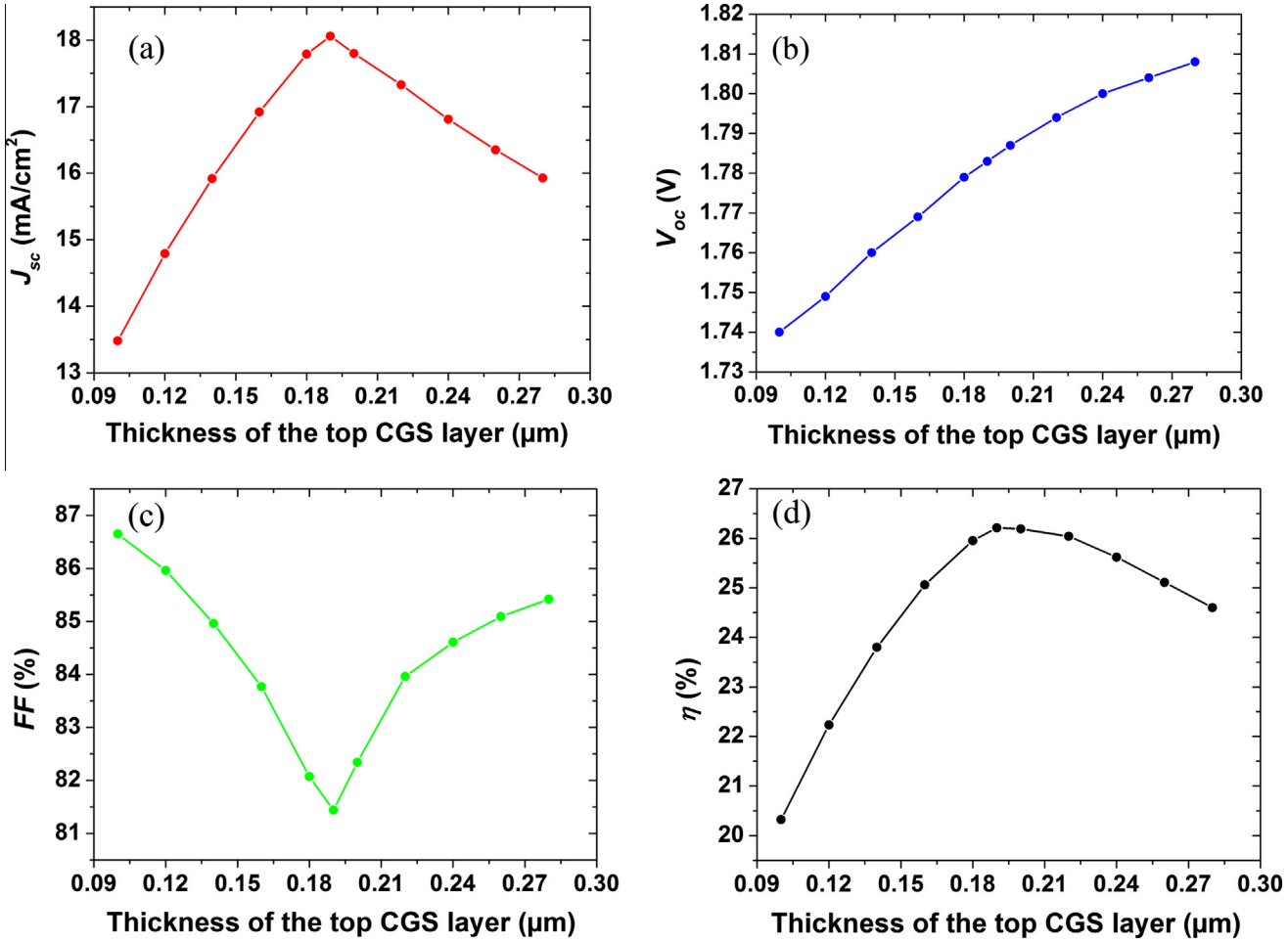

Fig. 7. Simulated photovoltaic parameters of the CGS/CIGS tandem solar cell as function of the top CGS layer thickness.

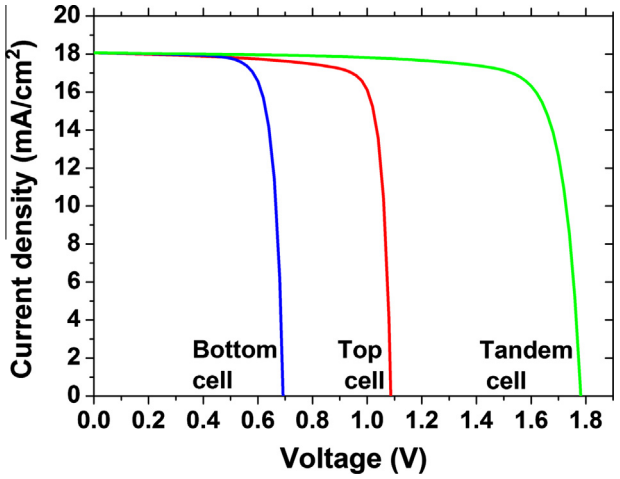

Fig. 8. J–V characteristics for the CGS top-cell, CIGS bottom-cell and CGS/CIGS tandem cell under short-circuit current densities matching.

Table 6
Optimized photovoltaic parameters of top, bottom and tandem solar cells under short-circuit current densities matching.

	J_{sc}(mA/cm^2)	V_{oc} (V)	FF (%)	η(%)
CGS top-cell	18.06	1.08	82.88	16.26
CIGS bottom-cell	18.06	0.7	79.46	9.93
CGS/CIGS tandem cell	18.06	1.78	82.88	26.21

Under current matching conditions at the optimal CGS layer thickness of 0.19 μm, the J–V characteristics of the top, bottom and tandem cells are plotted in Fig. 8. The photovoltaic parameters at the current matching point are summarized in Table 6. The short-circuit current densities of the top, bottom and tandem cells are all equal to the maximum J_{sc} 18.06 mA/cm^2. The open-circuit voltage V_{oc} of the tandem cell 1.78 V is equal to the sum of the V_{oc} of the top (1.08 V) and bottom (0.7 V) cells. The conversion efficiency of the tandem cell working at current matching condition is improved to 26.21% compared to the conversion efficiency 25.11% obtained for the CGS/CIGS tandem cell working at mismatched short-circuit current densities (Section 4.2).

5. Conclusion

Based on Silvaco–Atlas simulator, we presented numerical simulations to analyze the performance of single junction CIGS and CGS solar cells and a double junction CGS/CIGS tandem solar cell under AM1.5 G light spectrum. The J–V characteristics and associated PV parameters were determined. We first simulated separately optimized single junction CIGS and CGS solar cells and found, respectively, conversion efficiencies of about 20.32% and 18.92%, in good agreement with high record experimentally determined efficiencies. Then we studied the performance of a double junction CGS/CIGS tandem solar cell with the CGS as top-cell and the GIGS as bottom-cell. An enhancement of the conversion efficiency to 25.11% was achieved for a CGS/CIGS structure with arbitrary normal thicknesses of the top and bottom cells. Lower short-circuit current limitation and open-circuit voltage superimposition characteristics of the series connection of the top and bottom cells are demonstrated. Finally, we considered the thickness of the top-cell (CGS layer) as a key parameter to further improve the performance of the CGS/CIGS tandem cell. With fixed thickness of the bottom-cell (CIGS layer) at 3.5 μm, maximization of the CGS/CIGS tandem cell efficiency at 26.21% is achieved at an optimal thickness of the top-cell (CGS layer) of 0.19 μm. The condition of "current matching" where the top, bottom and tandem cells share the same short-circuit current density of 18.06 mA/cm^2, which is also the maximum of the tandem cell short-circuit current density at the optimal thickness 0.19 μm, is to be satisfied for the efficiency maximization. Thickness dependent top-cell (CGS layer) light absorption is essentially behind such CGS/CIGS tandem cell photovoltaic behaviour.

References

Amin, N., Tang, M., Sopian, K., 2007. Numerical modeling of the copper–indium–selenium (CIS) based solar cell performance by AMPS-1D. In: Proc. IEEE 5th Student Conference on Research and Development, Malaysia, pp. 1–6.

ATLAS User's Manual, Device Simulation Software, Version 5.20.2.R, SILVACO International, Santa Clara, CA, 2015.

Beiley, Z., Bowring, A., McGehee, M.D., 2012. Modeling low-cost hybrid tandem photovoltaics with power conversion efficiencies exceeding 20%. In: Proc. 38th IEEE Photovoltaic Specialists Conference, Austin, TX, USA, pp. 3129–3130.

Burdick, J., Glatfelter, T., 1986. Spectral response and IV measurements of tandem amorphous-silicon alloy solar cells. Sol. Cells 18, 301–314.

Chelvanathan, P., Hossain, M.I., Amin, N., 2010. Performance analysis of copper–indium–gallium–diselenide (CIGS) solar cells with various buffer layers by SCAPS. Curr. Appl. Phys. 10, S387–S391.

Cotal, H., Fetzer, C., Boisvert, J., Kinsey, G., King, R., Hebert, P., Yoon, H., Karam, N., 2009. III–V multijunction solar cells for concentrating photovoltaics. Energy Environ. Sci. 2 (2), 174–192.

Fotis, K., 2012. Modeling and simulation of a dual-junction CIGS solar cell using Silvaco Atlas, Monterey, California, Naval Postgraduate School.

Gloeckler, M., Fahrenbruch, A.L., Sites, J.R., 2003. Numerical modeling of CIGS and CdTe solar cells: setting the baseline. In: Proc. of Third World Conference on Photovoltaic energy Conversion, Osaka, Japan, pp. 491–94.

Green, M.A., 2001. Third generation photovoltaics: ultra-high conversion efficiency at low cost. Prog. Photovoltaics Res. Appl. 9, 123–135.

Green, M.A., Emery, K., Hishikawa, Y., Warta, W., Dunlop, E.D., 2013. Solar cell efficiency tables (version 42). Prog. Photovoltaics Res. Appl. 21, 827–837.

Huang, C.H., 2008. Effects of Ga content on Cu(In, Ga)Se_2 solar cells studied by numerical modeling. J. Phys. Chem. Solids 69, 330–334.

Hunger, R., Pettenkofer, Chr., Scheer, R., 2001. Surface properties of (1 1 1), (0 0 1)-oriented epitaxial $CuInS_2$/Si films. Surf. Sci. 477, 76–93.

Jackson, P., Hariskos, D., Lotter, E., Paetel, S., Wuerz, R., Menner, R., Wischmann, W., Powalla, M., 2011. New world record efficiency for Cu(In, Ga)Se_2 thin-film solar cells beyond 20%. Prog. Photovoltaics Res. Appl. 19, 894–897.

Jankovic, N., 2012. Numerical simulations of N-type CdSe poly-TFT electrical characteristics with trap density models of Atlas/Silvaco. Microelectron. Reliab. 52, 2537–2541.

Jeong, W.-S., Lee, J.-W., Jung, S., Yun, J.H., Park, N.-G., 2011. Evaluation of external quantum efficiency of a 12.35% tandem solar cell comprising dye-sensitized and CIGS solar cells. Sol. Energy Mater. Sol. Cells 95, 3419–3423.

Jiyon, S., Sheng, S.L., Huang, C.H., Anderson, T.J., Crisalle, O.D., 2003. Modeling and simulation of a $CuGaSe_2$/Cu(In, Ga)Se_2 tandem solar cell. In: Proc. 3rd World Conference on Photovoltaic Energy Conversion, Osaka, Japan, pp. 555–558.

Jun, D.-H., Kim, C.Z., Kim, H., Shin, H.-B., Kang, H.K., Park, W.-K., Shin, K., Ko, C.G., 2009. The effects of growth temperature and substrate tilt Angle on GaInP/GaAs tandem solar cells. J. Semicond. Technol. Sci. 9 (2), 91–97.

Liska, P., Thampi, K.R., Gratzel, M., Bremaud, D., Rudmann, D., Upadhyaya, H.M., Tiwari, A.N., 2006. Nanocrystalline dye-sensitized solar cell/copper indium gallium selenide thin-film tandem showing greater than 15% conversion efficiency. Appl. Phys. Lett. 88, 203103.

Marika, E., 2012. Thin film solar cells: research in an industrial perspective. Ambio 41 (Suppl 2), 112–118.

Nakada, T., Kijima, S., Kuromiya, Y., Arai, R., Ishii, Y., Kawamura, N., Ishizaki, H., Yamada, N., 2006. Chalcopyrite thin-film tandem solar cells with 1.5 V open circuit-voltage. In: Proc. IEEE 4th World Conf. on Photovoltaic Energy Conversion, Waikoloa, HI, pp. 400–403.

Nishiwaki, S., Siebentritt, S., Walk, P., Lux-Steiner, M.C., 2003. A stacked chalcopyrite thin-film tandem solar cell with 1.2 V open-circuit voltage. Res. Appl. 11, 243–248.

Olson, J.M., Friedman, D.J., Kurtz, S., 2003. Handbook of Photovoltaic Science and Engineering, first ed. John Wiley and Sons, West Sussex.

Ouédraogo, S., Zougmoré, F., Ndjaka, J.M.B., 2014. Computational analysis of the effect of the surface defect layer (SDL) properties on Cu(In, Ga)Se_2-based solar cell performances. J. Phys. Chem. Solids 75, 688–695.

Palik, E.D., 1998. Handbook of Optical Constants of Solids III. Boston Academic press, San Diego, London.

Paulson, P.D., Birkmire, R.W., Shafarman, W.N., 2003. Optical characterization of $CuIn_{1-x}$ Ga_xSe_2 alloy thin films by spectroscopic ellipsometry. J. Appl. Phys. 94, 879–888.

Repins, I., Contreras, M.A., Egaas, B., DeHart, C., Scharf, J., Perkins, C. L., To, B., Noufi, R., 2008a. 19.9% efficient ZnO/CdS/$CuInGaSe_2$ solar cell with 81.2% fill factor. Prog. Photovoltaics Res. Appl. 16, 235–239.

Repins, I., Contreras, M.A., Romero, M., Yan, Y., Metzger, W., Li, J., Johnston, S., Egaas, B., DeHart, C., Scharf, J., 2008b. Characterization of 19.9% efficient CIGS absorbers. In: Proc. 33rd IEEE Photovoltaic Specialists Conference, San Diego, California, pp. 1–6.

Richter, M., Schubbert, C., Eraerds, P., Riedel, I., Keller, J., Parisi, J., Dalibor, T., Avellán-Hampe, A., 2013. Optical characterization and modeling of Cu(In, Ga)(Se, S)$_2$ solar cells with spectroscopic ellipsometry and coherent numerical simulation. Thin Solid Films 535, 331–335.

Scheer, R., 2011. Towards an electronic model for $CuIn_{1-x}Ga_xSe_2$ solar cells. Thin Solid Films 519, 7472–7475.

Seyrling, S., Bucheler, S., Chirila, A., Perrenoud, J., Wenger, S., Nakada, T., Gratzel, M., Tiwari, A.N., 2009. Development of multijunction thin film solar cells. In: Proc. 34th IEEE Photovoltaic Specialists Conference, Philadelphia, PA, pp. 622–625.

SILVACO, 2015. solarex12.in: Thin film tandem solar cell www.silvaco.com/examples/tcad/section45/example12/index.html.

Shang, X., Wang, Z., Li, M., Zhang, L., Fang, J., Tai, J., He, Y., 2014. A numerical simulation study of $CuInS_2$ solar cells. Thin Solid Films 550, 649–653.

Shockley, W., Queisser, H.J., 1961. Detailed balance limit of efficiency of p–n junction solar cells. J. Appl. Phys. 32, 510–519.

Song, S.H., Aydil, E.S., Campbell, S.A., 2015. Metal-oxide broken-gap tunnel junction for copper indium gallium diselenide tandem solar cells. Sol. Energy Mater. Sol. Cells 133, 133–142.

Wang, W.L., Lin, H., Zhang, J., Li, X., Yamada, A., Konagai, M., Li, J. B., 2010. Experimental and simulation analysis of the dye sensitized solar cell/Cu(In, Ga)Se_2 solar cell tandem structure. Sol. Energy Mater. Sol. Cells 94, 1753–1758.

Xiao, Y.G., Li, Z.Q., Lestrade, M., Simon Li, Z.M., 2010. Modeling of CdZnTe and CIGS and tandem solar cells. In: Proc. 35th IEEE Photovoltaic Specialists Conference, Honolulu, HI, pp. 1990–1994.